Wenwu Zhang*

Y. Lawrence Yao

Department of Mechanical Engineering,
Columbia University, New York, NY 10027

I. C. Noyan

Thin Film Metallurgy Department, IBM T. J.
Watson Research Center,
Yorktown Heights, NY 10598

Microscale Laser Shock Peening of Thin Films, Part 1: Experiment, Modeling and Simulation

Microscale Laser Shock Peening (LSP), also known as Laser Shock Processing, is a technique that can be potentially applied to manipulate residual stress distributions in metal film structures and thus improve the fatigue performances of micro-devices made of such films. In this study, microscale LSP of copper films on single crystal silicon substrate is investigated. Before and after-process curvature measurement verifies that sizable compressive residual stress can be induced in copper thin films using microscale LSP. Improved modeling work of shock pressure is summarized and the computed shock pressure is used as loading in 3D stress/strain analysis of the layered film structure. Simulation shows that the stress/strain distribution in the metal film is close to equi-biaxial and is coupled into the silicon substrate. [DOI: 10.1115/1.1645878]

1 Introduction

More recently, reliability and failure problems in MEMS have attracted increasing attention [1,2]. While the dominant material in MEMS is silicon, metal and metallic thin film structures are often indispensable. Non-metal plates suffer from electrostatic stiction, which has become an important cause of MEMS failure. For metal structures, electrostatic stiction can be avoided and metal connection line can be integrated naturally with the metal structure. Aluminum thin film microwave switch was demonstrated to have very low current loss due to its small dimension and its metal structure [3]. These metallic thin film structures are typically made by patterning the thin film first and then sacrificing part of the supporting substrate.

Wearing of rubbing surfaces is the major cause of failure for silicon-based micro-engines [4], while tungsten-coated polysilicon micro-engines show much higher wear resistance than pure polysilicon structures [5]. The strength of silicon is determined by the integrity of the lattice. When defects or micro-cracks are present, the strength of silicon decreases sharply [6]. Thus, when the structure is irregular or when the aspect ratio of the structure is high, high quality lithography of silicon is difficult to achieve and defects in the structure may lead to serious reliability problems. Thicker microstructures ($>$10 microns) and higher aspect-ratio microstructure can be more economically and conveniently fabricated using electroforming (electroplating) techniques [7,8]. Wei et al. [9] demonstrated that high aspect ratio and complex geometry nickel microstructures could be obtained using electroforming techniques. Electroforming (electroplating) techniques are primarily for metals.

Some of these metal microstructures, such as micro-electromechanical actuators, metal gears, and metal switches, experience cyclic loads in service. Wear resistance and fatigue performance of these metal structures should be improved to increase the reliability of the system. Microscale Laser Shock Peening (LSP), also known as Laser Shock processing, has been shown to efficiently induce favorable residual stress distributions in bulk metal targets with micron-level spatial resolution [10,11]. It may potentially be used to improve the wear resistance and fatigue performance of metal film structures. The most popular metallic MEMS materials are copper, nickel and aluminum. Microscale LSP will not bring adverse effects to the micro-devices, since thermal effects are typically shielded by an ablative coating, and the water curtain typically used in LSP will carry away possible contamination of vaporized materials. Water does not have compatibility problems with MEMS materials and structures.

To apply microscale LSP to metallic components in microsystems, metallic films on silicon substrates need to be considered because LSP needs to be applied to the film before these components are patterned on the film and the silicon substrate is then partially sacrificed. It is necessary to understand how the thin film material on silicon substrate responds to LSP. The application of microscale LSP to metal films with a thickness less than 10 microns has not been studied in the literature. The microscale also poses challenges in terms of material characterization. Conventional X-ray diffractometry does not provide the spatial resolution necessary to characterize residual stress distribution with microscale resolution. Recent advances in X-ray microdiffraction offer promise and need to be investigated.

In Part 1 of this study, experiments of microscale LSP of copper thin films on silicon substrates are carried out. Preliminary curvature measurements prove that favorable compressive residual stress can be induced by microscale LSP. The improved modeling work of microscale LSP is described and simulation results of stress/strain analysis of layered thin film structures are presented. High-spatial resolution characterization of the stress/strain field in thin films will be presented in Part II of this study. X-ray microdiffraction [12] and instrumented nanoindentation [13] are used for the first time to measure the stress/strain variations in the shock treated thin films with micron-level spatial resolution.

2 Physical Phenomena in Laser Shock Processing

As illustrated in Fig. 1, when a short and intense ($>$1 GW/cm^2) laser pulse is irradiated onto a metallic surface, which is applied with a sacrificial coating (organic paint, tape, or thin metallic foil), the coating is instantaneously vaporized. The vapor absorbs the remaining laser light and produces a rapidly expanding plasma plume. This plasma induces shock waves during expansion from the irradiated surface, and a rapidly rising high-pressure shock wave propagates to the target. If the plasma is not confined, i.e., in open air, the pressure can only reach a fraction of 1 GPa. If confined by a water curtain or another medium, the shock pressure can be magnified by a factor of 5 or more compared with the open-air condition [14]. At the same time, the shock pressure lasts 2 to 3 times longer than the laser pulse duration. When the peak shock pressure is over the Hugoniot Elastic Limit (equivalent to the yield strength under shock conditions) for a suitable time, the metal yields and plastically deformed at the
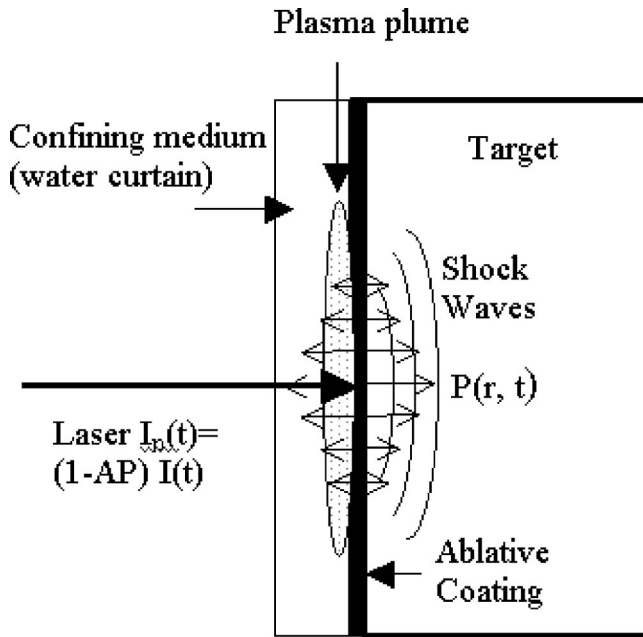
Fig. 1 Schematic of laser shock peening (LSP)

surface. As a result, in-plane compressive residual stress is induced. Surface hardness is also improved as a result of the plastic deformation. The coating used in LSP also prevents any melting of the target metal surface and thus the metal is ''cold worked.'' LSP is primarily a mechanical process rather than a thermal treatment.

3 Average Stress Measurement Using the Wafer Curvature Method

Curvature measurements are carried out to answer the question of whether microscale LSP can induce compressive residual stress in metal thin films. The samples are 1 μm and 3 μm thickness copper films on 1 in. round single crystal silicon wafers with (001) orientation and 0.254 mm thickness. The 1 μm samples are prepared by PVD at a chamber pressure of 2 mTorr. The 3 μm samples are prepared by electro plating. A Q-switched Nd:YAG laser with pulse duration of 50 ns and wavelength of 355 nm is used in the shock experiments. The laser beam diameter is about 12 microns. During laser shock processing, the sample is covered with an aluminum foil of 16 μm thickness, with a very thin layer of vacuum grease in between. Thus, thermal effects are largely isolated from the sample and only shock effects are experienced by the sample.

Shocks are applied along six parallel lines (10 mm in length and 2 mm in spacing) at the central part of a sample, and three laser pulses (pulse energy = 244 μJ) are applied at each location along the lines and these locations are 25 μm apart. The curvatures of the wafers before and after thin film deposition, as well as after laser shock peening are measured using an optical profiler (Model Wyko 3300). Knowing the curvature, the average residual stress in the thin film on the silicon substrate can be calculated according to [15]:

$$\sigma_f = \frac{M_s t_s^2}{6 t_f} (1/R - 1/R_0) \qquad (1)$$

where t_s and t_f are the thickness of the substrate and the film, respectively, $1/R$ and $1/R_0$ the current and original wafer curvature (seen from the film side), respectively, and M_s the biaxial modulus of the substrate. For the (001) single crystal silicon wafer, $M_s = 180.5$ GPa [15]. Equation (1) applies under the assump-
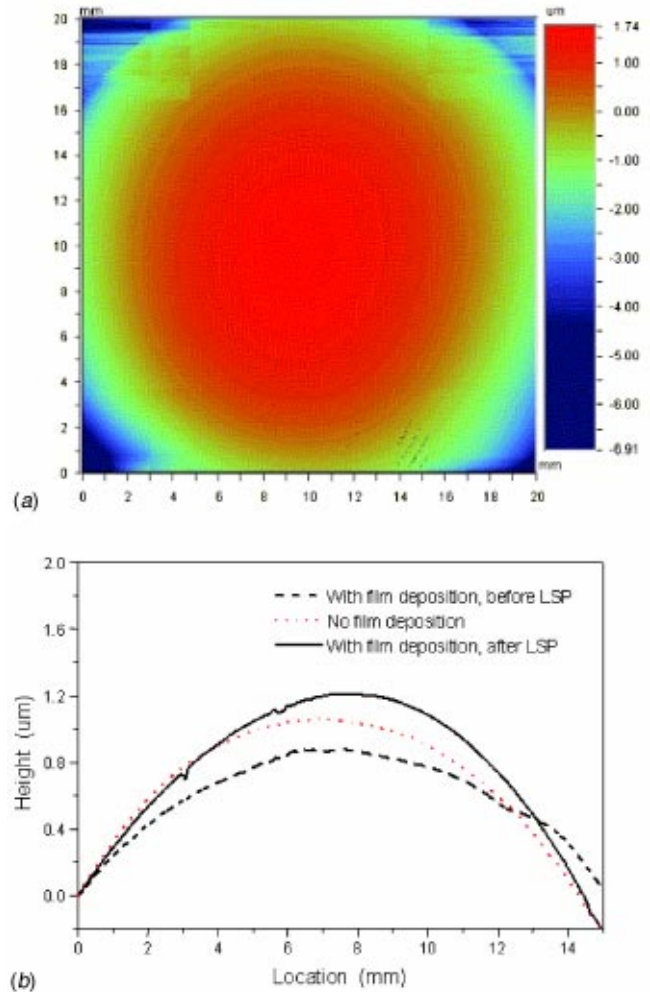

Fig. 2 Typical curvature measurement of 1 μm-thick copper film on silicon substrate (a) 2D contour plot of the sample surface height, after LSP; and (b) Surface profile variations.

tion of small deformation and pure elastic bending of a thin plate. Furthermore, it is assumed that the residual stress is uniform throughout the depth of the film [16].

Figure 2(a) shows the 2D contours of the 1 μm sample after LSP measured with the optical profiler. Curvature of the wafer can be measured from the profiles, as shown in Fig. 2(b). Copper has a larger expansion coefficient than silicon. After film deposition and cooling down, the copper film contracts more than the silicon substrate. Thus, the copper film experiences tensile stress and thus the substrate close to the film experiences compressive stress. As a result, the initially convex curvature of the wafer becomes less convex after film deposition. It becomes more convex again after LSP due to LSP induced compressive residual stress in the film.

Using Eq. (1), the residual stress variations in the thin films are computed and shown in Table 1. Both 1 μm and 3 μm samples show tensile residual stresses after film deposition, and both change to compressive after laser shock peening. The film stress after LSP increases significantly with the increase in film thickness. For the 1 μm samples, the change is $-35.4 - (31) = -66.4$ MPa, while for 3 μm samples, the change is -314.17 MPa. This is because there is more time for shock wave to propagate and compress a thicker film than a thinner one. Considering that only six lines of shock loads are applied on the film surface, it is concluded that microscale LSP can induce substantial compressive residual stresses in metal thin films on silicon substrates.

Table 1   Results of curvature measurement. Curvature change $=(1/R-1/R_0)$, unit 1/m.

Film type	Curvature with no film deposition	Curvature after film deposition but before LSP		Curvature after film deposition and after LSP	
		$(1/R-1/R_0)$	Stress	$(1/R-1/R_0)$	Stress
1 μm	−0.0445	0.016	+31 MPa	−0.0182	−35.40 MPa
3 μm	−0.0272	0.3597	+249.7 MPa	−0.1053	−64.47 MPa

Curvature measurement can only estimate the average stress in the thin film. To study the local distribution of the stress/strain field, however, modeling work and high spatial resolution experimental work are carried out.

4   Improved Modeling of Laser Induced Shock Pressure

The modeling work of LSP consists of the modeling of shock pressure and the modeling of stress/strain evolution. Laser shock processing of metals involves high strain rate and high shock pressure. In the stress analysis of LSP, work hardening, strain rate and pressure effects on the yield strength of metals are considered similarly as in [11] and will not be repeated here. The improved modeling of shock pressure will be discussed in this section.

4.1   Limitations of Existing LSP Models.   The shock pressure models of Clauer et al. [17] and Fabbro et al. [18] assume that the laser irradiation is uniform and therefore shock propagation in the confining medium and the target is one-dimensional. The 1-D assumption is appropriate when the size of a laser beam, whose intensity typically follows a Gaussian distribution, is relatively large. The shock model of Zhang and Yao [10] made simple modifications to Fabbro's model to account for the micro scale concerned by preserving the 1-D assumption while considering a 2-D (axisymmetric) equivalence.

The above shock pressure models assume that a certain amount of plasma exists instantaneously once laser is on. In reality, laser irradiation first vaporizes the surface layer of the coating, and the vaporized material quickly evolves into plasma. Water near the plasma outer edge is quickly ionized and becomes strongly absorbent to the incident laser irradiation. At the same time, the coating is continuously vaporized into the plasma. Explicit consideration of the mass transfer in the LSP system will eliminate the need for prescribing the value of α, the fraction of plasma internal energy used to increase the pressure of plasma, and thus increase the model accuracy, which is crucial for the micro scale under consideration. In addition, radial expansion of plasma can no longer be neglected in the micro-scale LSP modeling since it is in the same order of the small beam size. Some improvement in the modeling work of shock pressure as applied to bulk materials is presented in [19]. More details are presented below.

4.2   Improved Modeling of Laser Induced Shock Pressure. Under typical conditions of LSP, the speed of plasma expansion is lower than the shock speed, thus the shock wave precedes plasma expansion. This resembles the case of a laser supported combustion (LSC) wave [20]. LSC wave in air and vacuum has been studied [21] and is extended to LSP modeling.

In laser shock peening, water converts into plasma due to plasma and laser induced water breakdown [22]. At the same time, the coating is continuously vaporized and converted into plasma. Mass, momentum and energy are conserved across the shock wave. To model the process, the following assumptions are made: (1) Plasma expands only in the axial direction in the early stage, density, internal energy and pressure of the plasma are uniform within the plasma volume but can vary with time; (2) Plasma obeys ideal gas laws; (3) Only the coating layer is vaporized, the metal target experiences negligible thermal effects; and (4) The

coating layer is thin and well coupled with the metal target, thus the shock pressure and the particle velocities of the coating layer and the metal target are equal.

Let subscripts w denote water, m metal, c the coating layer, p plasma, L the side of plasma near water, R the side of plasma near solid, and 0 the property of unshocked region. Also let D be shock velocity, U particle velocity, E internal energy, ρ density, and P pressure. For convenience, the water-plasma-target system is divided into six regions (Fig. 3): unshocked water, shocked water, plasma, coating layer, shocked solid, and unshocked solid. The unshocked properties are known. The shocked and unshocked properties of water are related by mass, momentum, and energy conservation, and shock speed constitutive relations:

$$\rho_{w0}/\rho_w = 1-(U_w-U_{w0})/(D_w-U_{w0}) \tag{2}$$

$$P_w-P_{w0}=\rho_{w0}(D_w-U_{w0})(U_w-U_{w0}) \tag{3}$$

$$(E_w+U_w^2/2)-(E_{w0}+U_{w0}^2/2)=\frac{1}{2}(P_w+P_{w0})\left(\frac{1}{\rho_{w0}}-\frac{1}{\rho_w}\right) \tag{4}$$

$$D_w=D_{w0}+S_wU_w \tag{5}$$

For water, $U_{w0}=0$ m/s, $P_{w0}=10^5$ Pa, $E_{w0}=0$ J/kg, $\rho_{w0}=997.9$ kg/m^3, $D_{w0}=2,393$ m/s, and $S_w=1.333$ [23]. S_w is a coefficient relating shock speed D_w to U_w, the particle velocity and D_{w0}, the shock speed at infinitesimally small particle velocity. Substituting subscript m for w in Eqs. 2–5, one obtains four more equations between shocked and unshocked properties of metals. $U_{m0}=0$ m/s, $P_{m0}=10^5$ Pa, $E_{m0}=0$ J/kg. For copper, $\rho_{m0}=8,939$ kg/m^3, $D_{m0}=3,933$ m/s, and $S_m=1.489$ [24]. Mass and momentum conservation at the interfaces of water-plasma-metal at any instant requires:

$$\rho_w(U_{pL}-U_w)=\rho_pU_{pL} \tag{6}$$

$$\rho_c(U_{pR}-U_c)=\rho_cVrec=\rho_pU_{pR} \tag{7}$$

$$P_p+\rho_pU_{pR}U_c=P_c \tag{8}$$

$$P_p+\rho_pU_{pR}U_w=P_w \tag{9}$$

The current mass of the plasma is equal to the integration of the mass flows into plasma. The mass conservation of plasma requires:
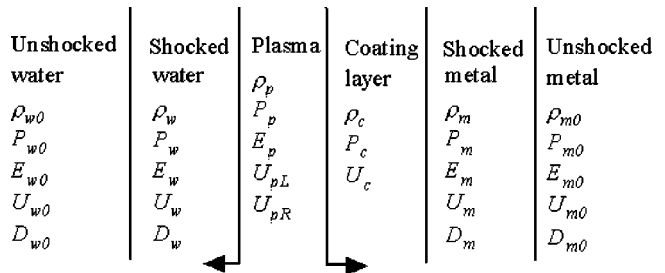
Unshocked water	Shocked water	Plasma	Coating layer	Shocked metal	Unshocked metal
ρ_{w0}	ρ_w	ρ_p	ρ_c	ρ_m	ρ_{m0}
P_{w0}	P_w	P_p	P_c	P_m	P_{m0}
E_{w0}	E_w	E_p	U_c	E_m	E_{m0}
U_{w0}	U_w	U_{pL}		U_m	U_{m0}
D_{w0}	D_w	U_{pR}		D_m	D_{m0}

Fig. 3   Six regions in LSP modeling

$$\rho_P(t)\int_0^t (U_{pL}+U_{pR})dt = \int_0^t (MF_w+MF_c)dt \qquad (10)$$

where MF_w is the mass flow from water into plasma, and MF_c the mass flow from the coating into plasma. The energy conservation of plasma considers the absorption of incident laser irradiation, E_{pt} the total energy stored in the plasma, W_p the work done by the plasma, and E_{MF} the energy exchanges through mass flow. The total energy of plasma consists of kinetic energy and internal energy, and using the ideal gas law, the internal energy of plasma is related to its density, specific heat ratio γ (about 1.3), and pressure. Let AP be the fraction of laser energy absorbed by plasma, and $I(t)$ the laser intensity, the energy conservation of plasma requires:

$$E_{pt}+W_p-E_{MF}=\int_0^t AP\times I(t)dt \qquad (11)$$

AP can be decided from experiments. Now the equations of this 1D shock pressure model are closed and all the variables involved can be solved as a function of time. Radial expansion of plasma is a more significant concern in micro-scale LSP than in mm-scale LSP because such expansion may not be neglected due to the small beam size. Once plasma is created, radial expansion of plasma commences. A rarefaction wave propagates into the plasma from the edge at the sound speed of the plasma. After a characteristic time $T_r=R_0/a$, where R_0 is the radius of the laser beam and a is the sound speed of the plasma, the rarefaction wave coalesces at the center of the spot. The pressure of the plasma drops and deviates from the 1D values afterwards. Axial relaxation starts after the laser pulse terminates, thus the characteristic time for axial expansion is $T_z=T_p$, where T_p is pulse duration. The temporal evolution of the plasma depends on the values of T_r and T_z. For the laser used in current research, $R_0=6$ microns, $T_z=T_p=50$ ns, and sound speed of plasma $a=300$ m/s, $T_r=20$ ns, thus radial relaxation occurs earlier than axial relaxation. Based on the work of Pirri [21], and Root [20], the following power scaling laws are used:

$$t<T_r \qquad \begin{array}{c} P=P_{1D} \\ R=R_0 \end{array}$$

$$T_z>t>T_r \qquad \begin{array}{c} P=P_{1D}(t/T_r)^{-4/5} \\ R=R_0(t/T_r)^{1/2} \end{array}$$

$$t>T_z \qquad \begin{array}{c} P=P_{1D}(T_r/T_z)^{4/5}(T_z/t)^{6/5} \\ R=R_0(T_z/T_r)^{1/2}(T_z/t)^{-4/5} \end{array} \qquad (12)$$

where P_{1D} is the plasma pressure from 1D model described above.

For laser shock peening on micron scale, the spatial profile of the laser beam should be considered. Following the work of Zhang and Yao [10], shock pressure obeys Gaussian spatial distribution, but with its $1/e^2$ radius equals to $\sqrt{2}R(t)$, where $R(t)$ is the radius of plasma in Eq. (12). Let r be the radial distance from the center of the laser beam, the spatially uniform shock pressure $P(t)$ relates to the spatially nonuniform shock pressure as

$$P(r,t)=P(t)\exp\left(-\frac{r^2}{2R^2(t)}\right) \qquad (13)$$

4.3 Results of Shock Pressure Modeling. The evolution of mass flow from water into plasma is shown in Fig. 4(a), which also shows the laser intensity profile normalized to the peak intensity. It is observed that the mass flow peaks after laser intensity peaks. The reason is that even after the laser intensity peaks, the plasma irradiation sustains the mass flow for a period of time. As laser intensity increases, plasma accumulates more energy to irradiate. This is why it takes longer for the mass flow to peak when laser intensity increases. The mass flow from the coating layer
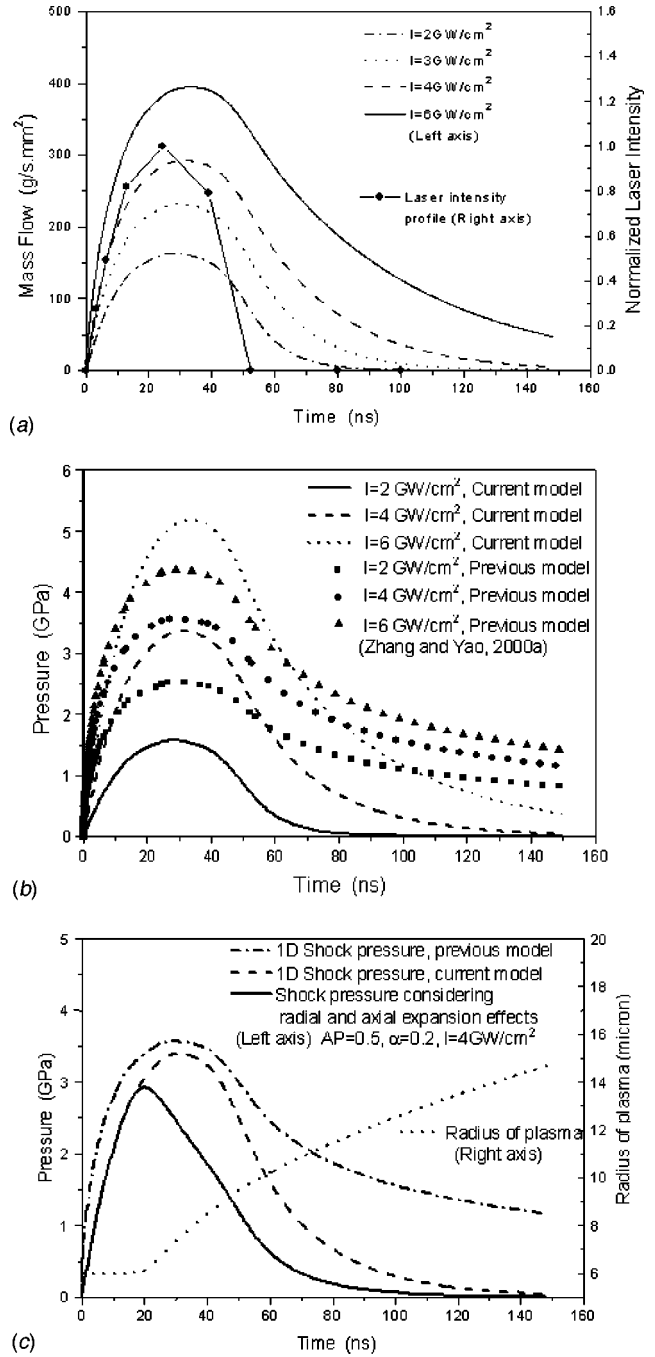

(a)

(b)

(c)

Fig. 4 (*a*) **Mass flow from water into plasma and normalized profile of laser intensity;** (*b*) **1D shock pressure comparison of current model and previous model [10]; and** (*c*) **Consideration of radial and axial expansion effects**

into plasma has similar features. The mass flows contribute to the evolution of plasma and the expansion of plasma imparts high shock pressures into water and target solid.

Figure 4(b) compares the 1D shock pressure determined using the current model and previous model [10]. The previous model assumes that a constant fraction $\alpha=0.2$ of plasma energy is used to increase the shock pressure. In the current model such conversion is inherently considered in the energy balance relations. As seen, the previous model determined a higher peak pressure at laser intensity of 2 GW/cm², a comparable value at 4 GW/cm², and a lower value at 6 GW/cm² than the current model. This is indicative of the shortcoming of using a constant value of α for

different laser intensities in the previous model. The pressures recover to zero values faster in the current model than in the previous model. The reason is that in the current model, plasma energy is used for the breakdown of water and target material besides the expansion of plasma, while in the previous model only the 1D expansion of plasma was considered.

The temporal evolution of shock pressure and the radius of plasma at laser intensity of 4 GW/cm² are shown in Fig. 4(c). A nonlinear increase of plasma radius occurs after 20 ns. The shock pressure deviates from the 1D results after the rarefaction wave merges at the beam center according to the power laws in Eq. (12). Obviously the shock pressure considering plasma expansion is more realistic and more suited for micro-scale LSP.

5 Stress/Strain Analysis

5.1 Special Considerations in the Simulation of Layered Thin Film Structures. 3D stress/strain analysis of copper thin films on silicon substrates is carried out using the shock pressure determined above as loading. The silicon substrate is treated as elastic and isotropic. The simulations are similar to previous 3D simulations of bulk metal foils [19], which were experimentally validated. But for thin film on silicon substrate, the interfacial phenomena require special considerations.

Stress/strain analysis of a layered structure should consider the stress coupling, contact condition and relative motion of the interfaces. Interfaces between dissimilar materials are susceptible to debonding and sliding, depending on the state of residual stress at the interface and the relative strength of the coating and the substrate [25]. Under tensile conditions, through-thickness cracks may develop and result in de-adhesion. Buckling can occur to compressed thin films on viscous deformable substrates, but not to ductile films in good binding with an elastic substrate such as single crystal silicon [26]. Laser shock processing is a dynamic process. Scheffler and Zukas [27] reviewed the general concerns in numerical simulation of dynamic events at material interfaces. Espinosa et al. [28] discussed in detail the contact/cohesive laws in the modeling of impact-induced delamination of composites. Cohesion and debonding are important when the interface is under tension and shear. When the interfaces are under compression and in contact, only the normal stress coupling and the tangential sliding need to be considered. Tangential sliding occurs when the shear stress at the interface exceeds the critical shear stress. The frictional shear stress τ is related to the normal stress σ_n (compressive) according to Coulomb's friction law:

$$\tau = \mu \sigma_n \quad (\sigma_n \text{ compressive}) \tag{14}$$

where μ is the friction coefficient. When the shear stress is less than the frictional shear stress, the interface remains intact, i.e., no sliding happens. When the shear stress exceeds the frictional shear stress, sliding happens and the tangential shear stress equals the frictional shear stress.

In this research, the samples were prepared through sputtering PVD and electro plating. The samples were carefully monitored to make sure that the films were well adhered to the substrates. In the experiments, all shock loads were applied to the central part of the film from the copper film side, and the normal stress at the interface is compressive most of the time. For this reason, no separation of interface occurred in any of the experiments. The high quality bonding in the central region of the film makes the tangential sliding very unlikely to occur. Thus, in simulations, tangential sliding is neglected, and the interfaces are assumed to be perfectly bonded. Across the interfaces, both displacement and normal stress are assumed to be continuous, that is,

$$S_{33,1} = S_{33,2}$$
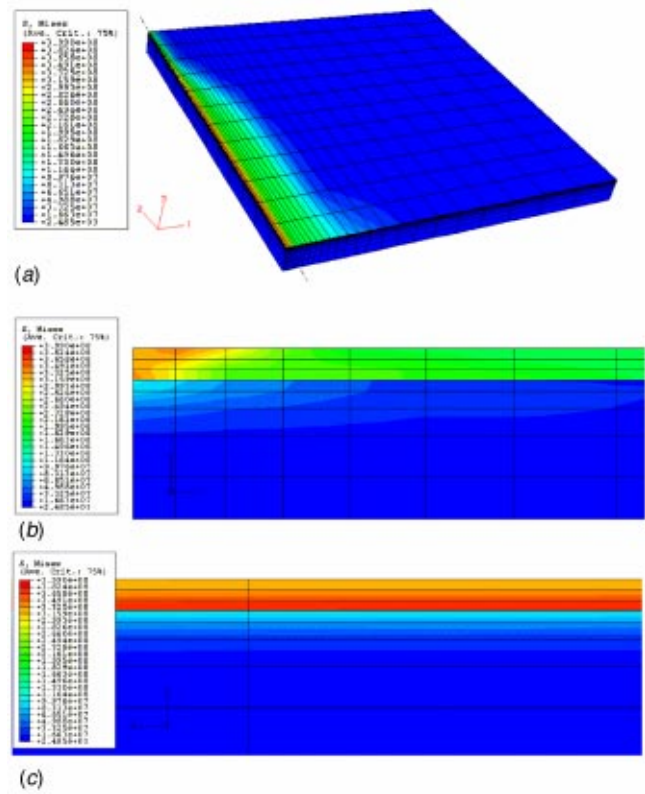
$$U_{i,1} = U_{i,2} \tag{15}$$

(a)

(b)

(c)

Fig. 5 Distribution of the von Mises stress, 1 μm-thick copper film on silicon substrate, pulse energy of 244 μJ (a) 3D overview (the dotted line denotes the symmetrical centerline); (b) detailed view of the interface along the cross section perpendicular to the centerline; and (c) detailed view of the interface along the centerline. For (a) the size is 200 microns in the 11-direction and 300 microns in the 22-direction, of which 225 microns were shock peened. For (b) and (c) only the elements close to the film-substrate interface are shown for viewing clarity.

where S_{33} is the normal stress, U_i the displacement, $i = 1,2,3$, and subscripts 1 and 2 denote the values across the interface. Interfaces in perfect contact obviate the need to consider the dynamic process in LSP additionally.

This interface algorithm is implemented in a commercial FEM package Abaqus. LSP is applied onto the copper film along a central line (the 22-direction) of a sample. Only a quarter of the shocked sample is computed due to symmetry, and the selected computation domain is 200 microns in the 11-direction and 300 microns (of which 225 microns shocked) in the 22-direction (Fig. 5(a)). The silicon substrate is 20 microns in thickness, while the copper thin film has a thickness of 1, 1.5 or 3 microns. Along the shocked line the spacing between consecutive laser pulses is 25 microns. The bottom surface of the silicon substrate is fixed in position. The two edges seen in Fig. 5(a) are symmetric about the 11 and 22-axes, respectively, and the two unseen edges are traction free.

5.2 Results and Discussion. Figure 5(a) shows the 3D von Mises stress distribution after laser shock processing of the 1 μm sample at pulse energy of 244 μJ and pulse diameter of 12 microns. The von Mises stress indicates the region of stress concentration. A line of shocks applied along the centerline of the sample influences a region about 75 microns on either side of the centerline. The stress/strain fields are approximately uniform along the 22-direction, except in the un-shocked region close to the far end of the centerline. Thus, a cross section profile in the following analysis can reflect the stress/strain distributions in the sample.
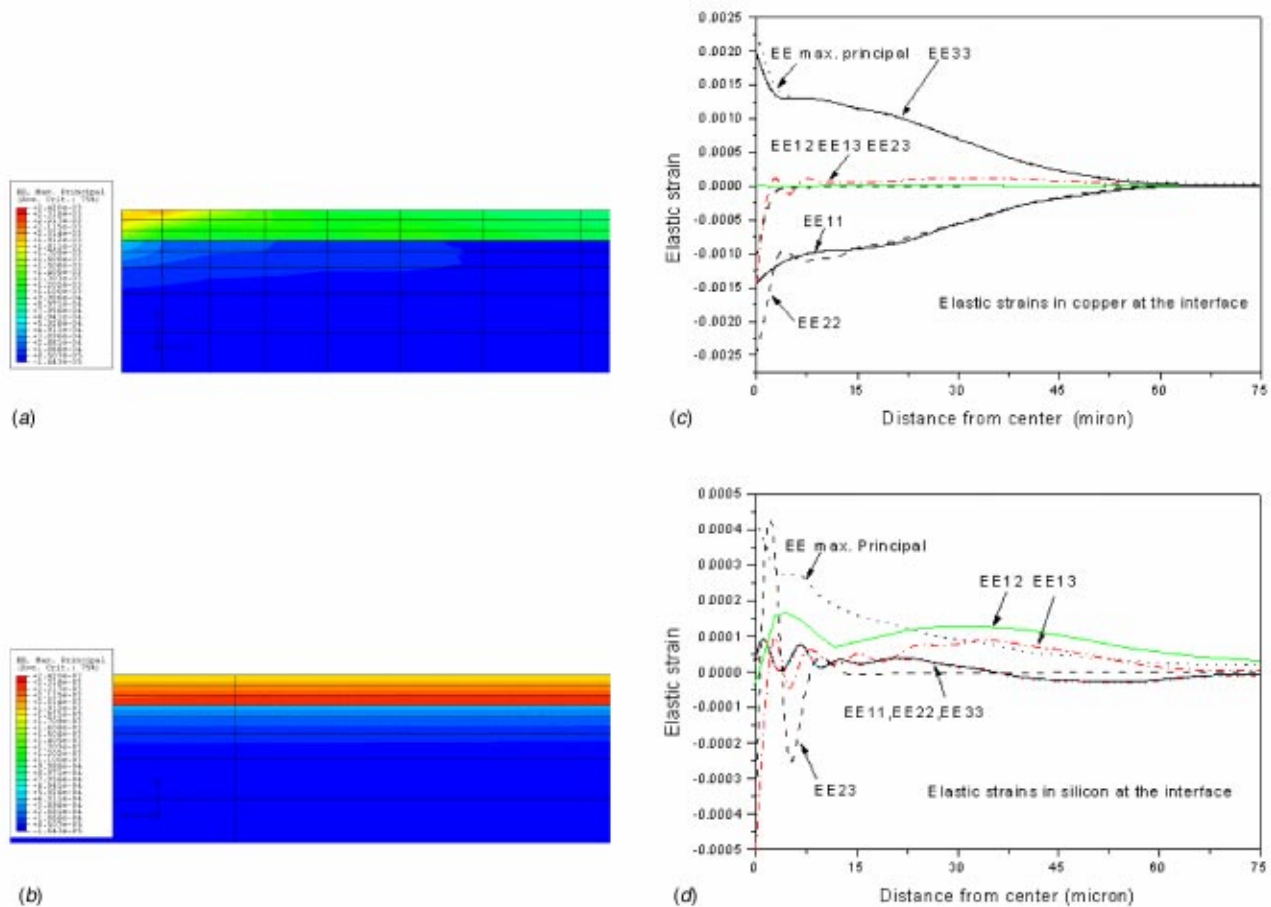
Fig. 6 Strain coupling at the copper-silicon interface, 1 μm-thick copper film on silicon substrate, pulse energy of 244 μJ (*a*) distribution of the maximum principal elastic strain along the cross section perpendicular to the centerline; and (*b*) distribution of the maximum principal elastic strain along the centerline; (*c*) variations of the elastic strain components in the copper film along the cross section; and (*d*) variations of the elastic strain components in the silicon substrate along the cross section. For (*a*) and (*b*) only the elements close to the film-substrate interface are shown for viewing clarity.

Stress/strain coupling at the interface is of special interest in order to understand the experimental results in X-ray diffraction measurement to be presented in Part 2 of this paper. Figure 5(*b*) shows in detail the stress coupling at the copper-silicon interface along the cross section perpendicular to the centerline. The top three elements are copper film. It is seen that the von Mises stress in the copper film concentrates in the region close to the center (around 10 microns). It becomes much smaller and almost uniform when away from the centerline but differs from that in the silicon substrate. This difference is not caused by LSP but rather by the film deposition process. Figure 5(*c*) shows the stress coupling along the centerline (the 22-direction). It is clear that stress at the same depth is nearly uniform along the 22-direction. Stress distribution in silicon spans a narrower range than in the copper film, and only a very thin layer (about 1 micron) of silicon near the interface is affected. The reason is as follows. After sufficient stress relaxation, the normal stress in the elastic silicon substrate is very small, but the silicon substrate experiences shear stress in the region close to the interface in order to balance the non-uniform residual stress in the copper film. The residual stress in the copper film becomes increasingly uniform when away from the center, thus, in the silicon the shear stress needed to balance the stress non-uniformity decreases quickly as the distance from the center increases. Shear stress induces elastic deformation in the silicon.

The strain coupling at the interface is studied in Figures 6(*a*). and 6(*b*) illustrate the distribution of maximum principal elastic

strain at the interface along the centerline and the cross section, respectively. The strain tensor has 6 components and maximum principal elastic strain is selected to reflect the variation of elastic strain concentration across the interface. Strains are coupled across the copper-silicon interface and similar trends in principal elastic strain variation are observed as in von Mises stress. Figures 6(*c*) and (*d*) show quantitatively the variation of individual strain components along the cross section at the interface in copper film and in silicon, respectively. In the copper film the normal strains are dominant, while the shear strains are very small, except in a narrow region close to the center. $EE11$ and $EE22$ are approximately equal except in the narrow region close to the center, and $EE33$ almost coincides with the maximum principal elastic strain. Thus, the strain distribution in thin film is nearly equi-biaxial. From Fig. 6(*d*) it is clear that in silicon the normal strains are weak compared with the shear strains. The shear stress or shear strain in silicon is due to the nonuniformity of stress/strain in the copper layer at the interface. Silicon has a higher Young's modulus than copper (180.5 GPa vs. 126 GPa); thus, under the same level of stress, the strain values in the silicon are smaller than those in the copper. The variation of strain components in the silicon is complex. However, maximum principal elastic strain captures the trend of elastic strain concentration in silicon.

Simulation results in Fig. 7(*a*) show that on the top surface along the cross section (perpendicular to the center line) of the sample, the values of stress $S11$ and $S22$ are close to each other, and $S33$ is nearly zero everywhere. Thus, the stress distribution in

Fig. 8 X-ray diffraction intensity contrast measurement across the shocked region measured in 2-micron step size. 244 μJ and 209 μJ, 1 μm-thick copper film on silicon substrate. The diffraction intensity is normalized to the average background diffraction intensity (14000 counts).
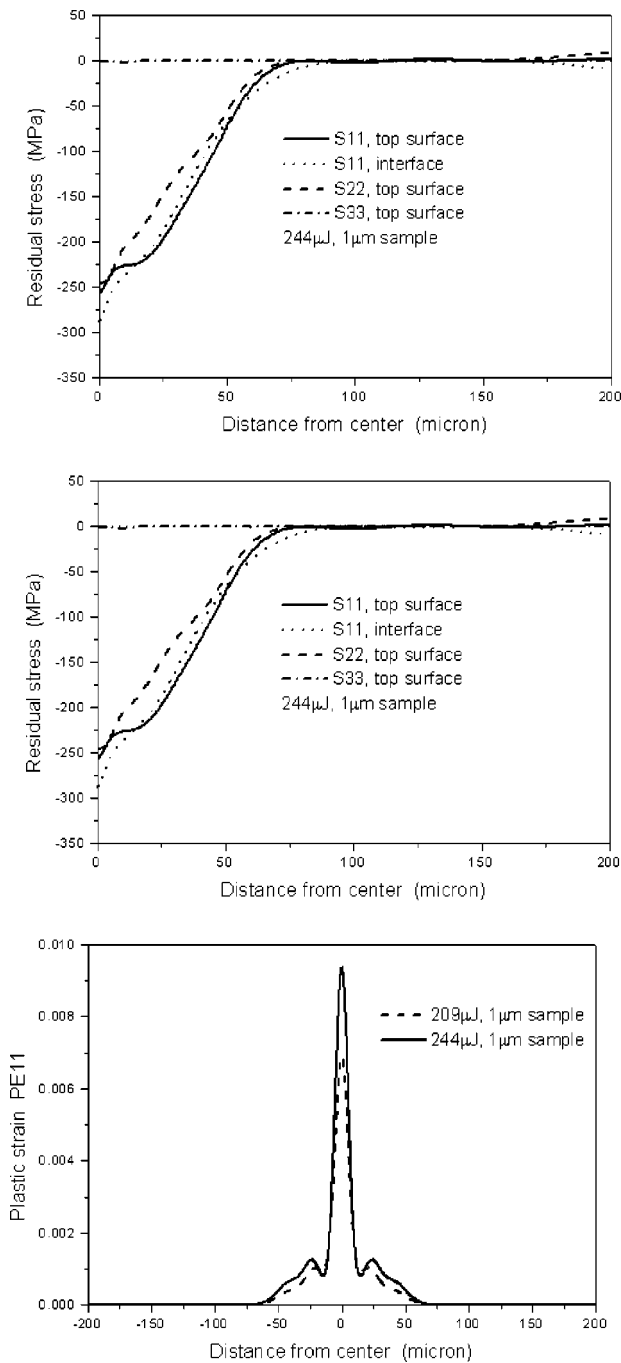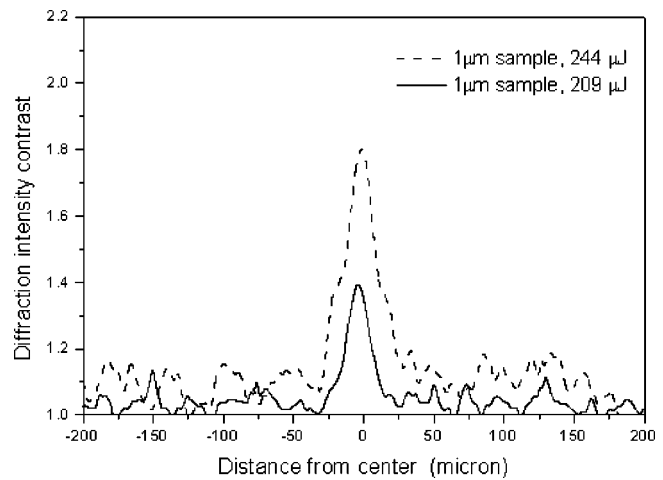

Fig. 7 Stress/strain simulation results, 1 μm-thick copper film on silicon substrate (*a*) Distribution of residual stresses across the shocked region, pulse energy 244 μJ; (*b*) Comparison of S11 at 244 and 209 μJ; and (*c*) Comparison of plastic strain PE11 at 244 and 209 uJ.

the film is close to equi-biaxial. The value of S11 at the interface is compared with the value on the top surface. It is seen that except in a narrow range near the centerline ($<$10 microns), S11 is nearly uniform throughout the depth of the film. The distributions of top-surface residual stress S11 for the 1 μm sample at pulse energy of 244 μJ (4.31 GW/cm^2) and 209 μJ (3.67 GW/cm^2) are compared in Fig. 7(*b*). Within 50 microns from the center, the in-plane stress is compressive and larger than 100 MPa. Although the increase of compressive residual stress (-225 to -250 MPa) is not substantial when the energy is increased from 209 μJ to 244 μJ, plastic strain PE11 has a more

substantial increase as seen in Fig. 7(*c*). In fact, plastic strain PE22 (not shown) in the copper film is nearly equal to PE11. Thus, the increased energy is dissipated through plastic deformation while does not increase the residual stress substantially.

The shock-induced stress/strain simulation results above are experimentally investigated and validated using the X-ray microdiffraction technique [12] which gives micron-level spatial resolution. The conventional X-ray diffraction gives spatial resolution in the order of millimeters. The higher spatial resolution is necessary in order to characterize the stress/strain field induced by microscale LSP in which the region affected by a laser beam of diameter 10 microns is about 50 to 75 microns. The principle of this measurement will be detailed in Part 2 of this paper. Very briefly, instead of directly measuring the strain in the copper thin film, which is only a couple of microns thick, diffraction from the silicon substrate is measured. The stress/strain coupling from the copper film deforms the single crystal silicon substrate. This transition from nearly perfect crystal to imperfect crystal results in X-ray diffraction intensity increase when the X-ray microbeam scans across the shocked region and penetrates the top thin film layer, and the diffraction intensity of the single crystal substrate is recorded. Figure 8 shows typical profiles of Si (004) diffraction intensity contrast along the cross section of the shocked line on a 1 μm-thick thin film sample. The diffraction intensity is normalized to the background diffraction intensity. All the measurements were taken at 2 microns spacing. Although some fluctuations exist in the diffraction profile, large central peaks were prominently seen for both 244 μJ and 209 μJ pulse energy, and the magnitude agrees with the trend in simulation: the higher the diffraction intensity, the stronger the shock load. The peaks are 1.8 and 1.4 for 244 μJ and 209 μJ, respectively, while the half-widths of the peaks are 30–40 microns, which agree with the simulation results. For both cases, the X-ray intensity contrast reflects the stress/strain concentration in the shocked region. The correlations between these experimental results and the simulation results will be further discussed in Part 2 of this paper.

6 Conclusions

Microscale laser shock peening can induce compressive in-plane residual stress in copper thin film on silicon substrate as shown by the wafer curvature measurements and 3D stress/strain simulations. The compressive residual stress distribution is beneficial for the prevention of micro-crack initiation and propagation. 3D simulations based on an improved shock pressure model

confirm that the stress/strain distribution in the thin film is nearly equi-biaxial. The stress/strain field in the thin film is coupled to the silicon substrate and the silicon substrate is elastically deformed in the shock-affected region. These results will be used to interpret and compare with the results of high spatial resolution measurements of the stress/strain fields in Part II of this paper.

References

[1] Miller, S. L., Rodgers, M. S., LaVigine, G., Sniegowski, J. J., Clews, P., Tanner, D. M., and Peterson, K. A., 1998, "Failure Modes in Surface Micromachined Micro-Electro-Mechanical Actuators," *IEEE 98CH36173, 36th Annual International Reliability Physics Symposium*, pp. 17–25.

[2] Tanner, D. M., Walraven, J. A., Helgesen, K. S., Irwin, L. W., Gregory, D. L., Stake, J. R., and Smith, N. F., 2000, "MEMS Reliability in a Vibration Environment," *IEEE 00CH37059, 38th Annual International Reliability Physics Symposium*, pp. 139–145.

[3] Chang, C., and Chang, P., 2000, "Innovative Micromachined Microwave Switch with Very Low Insertion Loss," Sens. Actuators A, **79**(1), Jan., pp. 71–75.

[4] Tanner, D. M., Miller, W. M., Peterson, K. A., Dugger, M. T., Eaton, W. P., Irwin, L. W., Senft, D. C., Smith, N. F., Tangyunyong, P., and Miller, S. L., 1999, "Frequency Dependence of the Lifetime of a Surface Micromachined Microengine Driving a Load," Microelectron. Reliab., **39**(3), pp. 401–414.

[5] Walraven, J. A., Mani, S. S., Fleming, J. G., Headley, T. J., Kotula, P. G., Pimentel, A. A., Rye, M. J., Tanner, D. M., and Smith, N. F., 2000, "Failure Analysis of Tungsten Coated Polysilicon Micromachined Microengines," *MEMS Reliability for Critical Applications, Proceedings of SPIE*, Vol. 4180, pp. 49–57.

[6] Petersen, Kurt E., 1982, "Silicon as a Mechanical Material," Proc. IEEE, **70**(5), pp. 420–457.

[7] Johansen, L. S., Ginnerup, M., Ravnkilde, J. T., Tang, P. T., and Löchel, B., 2000, "Electroforming of 3D Microstructures on Highly Structured Surfaces," Sens. Actuators A, **83**(1–3), pp. 156–160.

[8] Hart, T., and Watson, A., 2000, "Electroforming," Metal Finishing, **98**(1), pp. 388–399.

[9] Wei, Z.-J. et al., 2000, "Study of Wetters in Nickel Electroforming of 3D Microstructures," Mater. Chem. Phys., **63**, pp. 235–239.

[10] Zhang, W., and Yao, Y. L., 2000, "Improvement of Laser Induced Residual Stress Distributions via Shock Waves," *Proc. ICALEO'00, Laser Materials Processing*, Vol. 89, pp. E183–192.

[11] Zhang, W., and Yao, Y. L., 2000b, "Micro Scale Laser Shock Processing of Metallic Components," ASME J. Manuf. Sci. Eng., **124**(2), May, pp. 369–378.

[12] Noyan, I. C., Jordan-Sweet, J. L., Liniger, E. G., and Kaldor, S. K., 1998, "Characterization of Substrate/Thin-film Interfaces with X-ray Microdiffraction," Appl. Phys. Lett., **72**(25), pp. 3338–3340.

[13] Suresh, S., and Giannakopoulos, A. E., 1998, "A New Method for Estimating Residual Stresses by Instrumented Sharp Indentation," Acta Mater., **46**, pp. 5755–5767.

[14] Fox, J. A., 1974, "Effect of Water and Paint Coatings on Laser-irradiated Targets," Appl. Phys. Lett., **24**(10), pp. 461–464.

[15] Segmüller, A., Angilelo, J., and La Placa, S. J., 1980, "Automatic X-ray Diffraction Measurement of the Lattice Curvature of Substrate Wafers for the Determination of Linear Strain Patterns," J. Appl. Phys., **51**(12), pp. 6224–6230.

[16] Stoney, G. G., 1909, "Metallic Films Deposited by Electrolysis," Proc. Royal Soc., **82**(535), pp. 172–175.

[17] Clauer, A. H., and Holbrook, J. H., 1981, "Effects of Laser Induced Shock Waves on Metals," *Shock Waves and High Strain Phenomena in Metals-Concepts and Applications*, New York, Plenum, pp. 675–702.

[18] Fabbro, R., Fournier, J., Ballard, P., Devaux, D., and Virmont, J., 1990, "Physical Study of Laser-produced Plasma in Confined Geometry," J. Appl. Phys., **68**(2), pp. 775–784.

[19] Zhang, W., and Yao, Y. L., 2001, "Modeling and Simulation Improvement in Laser Shock Processing," *Proc. ICALEO'2001*, Section A.

[20] Root, R. G., 1989, "Modeling of Post-breakdown Phenomena," *Laser Induced Plasmas and Application*, New York, Marcel Dekker, Inc., pp. 95–99.

[21] Pirri, A. N., 1978, "Plasma Energy Transfer to Metal Surfaces Irradiated by Pulsed Lasers," AIAA J., **16**(12), pp. 1296–1304.

[22] Vogel, A., Nahen, K., Theisen, D., and Noack, J., 1996, "Plasma Formation in Water by Picosecond and Nanosecond Nd:YAG Laser Pulses," IEEE J. Sel. Top. Quantum Electron., **2**(4), pp. 847–871.

[23] Assay, James R., and Shahipoor, M., 1992, *High-Pressure Shock Compression of Solids*, New York, Springer-Verlag, pp. 78–82.

[24] Meyer, L. W., 1992, "Constitutive Equations at High Strain Rates," *Shock Wave and High-Strain-Rate Phenomena in Metals*, New York, Marcel Dekker, Inc., pp. 49–68.

[25] Teixeira, V., 2001, "Mechanical Integrity in PVD Coatings due to the Presence of Residual Stresses," Thin Solid Films, **392**, pp. 276–281.

[26] Sridhar, N., Srolovitz, D. J., and Suo, Z., 2001, "Kinetics of Buckling of a Compressed Film on a Viscous Substrate," Appl. Phys. Lett., **78**(17), pp. 2482–2484.

[27] Scheffler, D. R., and Zukas, J. A., 2000, "Practical Aspects of Numerical Simulation of Dynamic Events: Material Interfaces," Int. J. Impact Eng., **24**, pp. 821–842.

[28] Espinosa, H. D., Dwivedi, S., and Lu, H.-C., 2000, "Modeling Impact Induced Delamination of Woven Fiber Reinforced Composites with Contact/Cohesive Laws," Comput. Methods Appl. Mech. Eng., **183**(3–4), pp. 259–290.